

PRODUCTION OF SECONDARIES IN SOFT p+Pb COLLISIONS AT LHC AND ALICE DATA

C. Merino, C. Pajares, and Yu. M. Shabelski*

Departamento de Física de Partículas, Facultade de Física,
and Instituto Galego de Física de Altas Enerxías (IGFAE),
Universidade de Santiago de Compostela, Galicia, Spain
E-mail: merino@fpaxp1.usc.es, pajares@fpaxp1.usc.es

* Permanent address: Petersburg Nuclear Physics Institute,
NCR Kurchatov Institute
Gatchina, St.Petersburg 188350 Russia
E-mail: shabelsk@thd.pnpi.spb.ru

A b s t r a c t

We calculate the inclusive spectra of secondaries produced in soft (minimum bias) p+Pb collisions in the framework of Quark-Gluon String Model at LHC energy, and by taking into account the inelastic screening corrections (percolation effects). The role of these effects is expected to be very large at very high energies, and they should decrease the spectra more than 1.5 times in the midrapidity region and increase them about 1.5 times in the fragmentation region at the energy of LHC.

PACS. 25.75.Dw Particle and resonance production

1 Introduction

The detailed investigation of p+Pb interactions at the highest LHC energy of $\sqrt{s} = 5$ TeV (4 TeV proton beam and $1.57 \cdot A$ TeV Pb beam) makes part of the nearest plans by LHC. The investigation of soft p+Pb interactions is very interesting because it can give the final answer to the problem of inelastic shadow corrections [1, 2] for inclusive particle production.

The recent data obtained by the ALICE Collaboration [3] confirm the existence of these corrections at the LHC energy. The magnitude of these inelastic shadow corrections corresponds to the resulting contribution of complicate Reggeon diagrams with multipomeron interaction [1].

In the present paper we present the predictions of the Quark-Gluon String Model (QGSM) [4, 5] for the rapidity and x_F distributions of secondaries produced in p+Pb at $\sqrt{s} = 5$ TeV. The QGSM quantitatively describes many features of high energy production processes, including the inclusive spectra of different secondary hadrons produced in high energy hadron-nucleon [6, 7, 8, 9], hadron-nucleus [10, 11], and nucleus-nucleus [12] collisions. The Monte Carlo version of QGSM is described in [13]. The model parameters used in the present calculations were fixed by comparison of the theoretical calculations to the experimental data.

In the case of interaction with a nuclear target the Multiple Scattering Theory (Gribov-Glauber Theory) is used, what allows to consider the interaction with the nuclear target as the superposition of interactions with different numbers of target nucleons. However, it was shown in [1, 2] that the description of the inclusive spectra of secondaries produced in d+Au collisions at $\sqrt{s} = 200$ GeV (RHIC) requires to account for the inelastic shadow corrections. These corrections are connected to the multipomeron interactions and they lead to the saturation of the inclusive density of secondary hadrons in the soft (low p_T) region, where the methods based on perturbative QCD cannot be used. The effects of the inelastic shadow corrections should increase with the initial energy. The difference in the calculations with and without these effects at LHC energies is of about 3 times in the midrapidity region and of about 2 times in the fragmentation region.

Other predictions for secondary production in p+Pb collisions at LHC energies (mainly for hard collisions can be found in [14, 15, 16, 17, 18].

2 Inclusive spectra of secondary hadrons in the Quark-Gluon String Model

In order to produce quantitative predictions a model for multiparticle production is needed. For that purpose we have used the QGSM [4, 5] in the numerical calculations presented below.

In the QGSM high energy hadron–nucleon and hadron–nucleus interactions are considered as proceeding via the exchange of one or several Pomerons, and all elastic and inelastic processes result from cutting through or between Pomerons [19]. Each Pomeron corresponds to a cylinder diagram (see Fig. 1a) that, when cutted, produces two showers of secondaries as it is shown in Fig. 1b. The inclusive spectrum of secondaries is determined by the convolution of diquark, valence quark, and sea quark distributions, $u(x, n)$, in the incident particles, with the fragmentation functions, $G(z)$, of quarks and diquarks into secondary hadrons. Both functions $u(x, n)$ and $G(z)$ are determined by the corresponding Reggeon diagrams [20].

The diquark and quark distribution functions depend on the number n of cut Pomerons in the considered diagram. There exists some freedom on how to share the initial energy among the Pomerons at $n > 1$ [10, 21]. In the following calculations we use the receipt of [10].

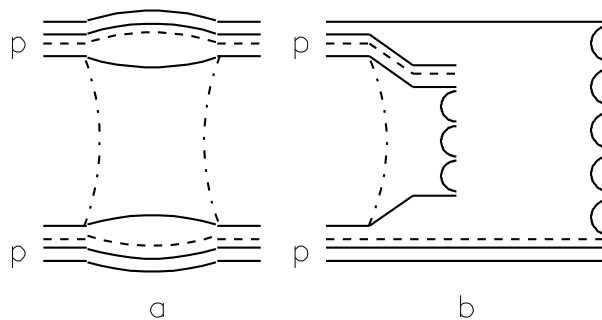


Figure 1: a) Cylinder diagram (cylinder is shown by dash-dotted curves) corresponding to the one–Pomeron exchange contribution to elastic pp scattering, b) and the corresponding cut diagram which represents its contribution to the inelastic pp cross section. Quarks are shown by solid curves and string junctions by dashed lines.

In the case of a nucleon target the inclusive spectrum of a secondary hadron h has the form [4]:

$$\frac{dn}{dy} = \frac{1}{\sigma_{inel}} \cdot \frac{d\sigma}{dy} = \frac{x_E}{\sigma_{inel}} \cdot \frac{d\sigma}{dx_F} = \sum_{n=1}^{\infty} w_n \cdot \phi_n^h(x) \quad , \quad (1)$$

where the functions $\phi_n^h(x)$ determine the contribution of diagrams with n cut Pomerons and w_n is the probability for this process to occur [22]. Here we neglect the diffraction dissociation contributions which are important mainly for the secondary production in the large x_F region that is not significant in the present calculations.

For pp collisions

$$\phi_n^h(x) = f_{qq}^h(x_+, n) \cdot f_q^h(x_-, n) + f_q^h(x_+, n) \cdot f_{qq}^h(x_-, n) + 2(n-1) f_s^h(x_+, n) \cdot f_s^h(x_-, n) \quad , \quad (2)$$

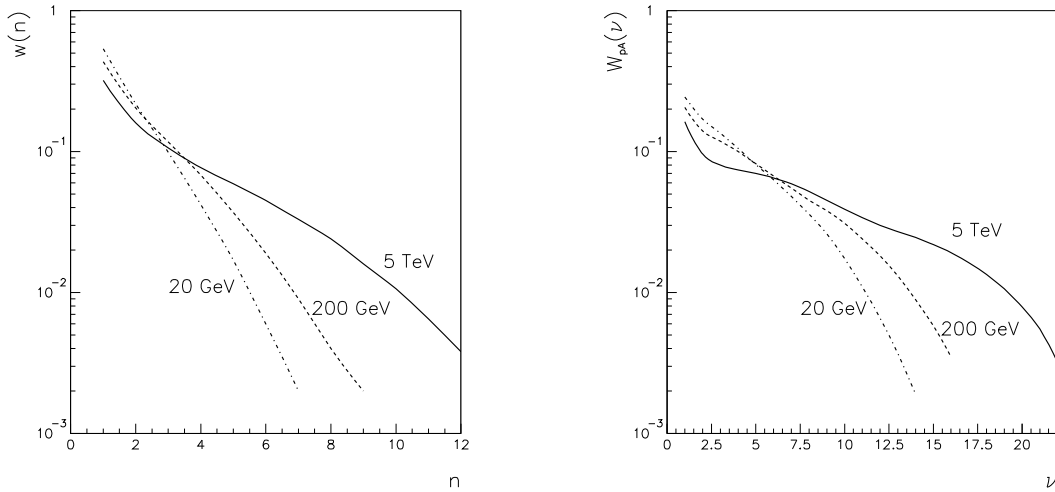


Figure 2: The distribution of probabilities to cut n Pomerons, w_n in pp interactions (left), and the distribution of probabilities for the inelastic interaction of a proton with ν lead nucleons, $W_{pPb}(\nu)$, in p+Pb interactions (right), at three initial energies, $\sqrt{s} = 5$ TeV (solid curves), 200 GeV (dashed curves), and 20 GeV (dash-dotted curves).

$$x_{\pm} = \frac{1}{2}[\sqrt{4m_T^2/s + x^2} \pm x] \quad , \quad (3)$$

where f_{qq} , f_q , and f_s correspond to the contributions of diquarks, valence quarks, and sea quarks, respectively.

These contributions are determined by the convolution of the diquark and quark distributions with the fragmentation functions, e.g.,

$$f_q^h(x_+, n) = \int_{x_+}^1 u_q(x_1, n) \cdot G_q^h(x_+/x_1) dx_1 \quad . \quad (4)$$

The diquark and quark distributions, as well as the fragmentation functions, are determined by Regge intercepts [20]. The numerical values of the model parameters were presented in ref. [7].

The probabilities w_n in Eq. (1) are the ratios of the cross sections corresponding to n cut Pomerons, $\sigma^{(n)}$, to the total non-diffractive inelastic pp cross section, σ_{nd} [22].

The contribution of multipomeron exchanges in high energy pp interactions results in a broad distribution of w_n . These distributions at three different energies $\sqrt{s} = 5$ TeV, 200 GeV, and 20 GeV are presented in the left panel of Fig. 2.

In the case of nuclear target (or colliding beam) a projectile proton can interact with several nucleons. Let $W_{pA}(\nu)$ be the probability for the inelastic interactions of the proton with ν nucleons and σ_{prod}^{pA} the total cross section of secondary production in a p+A collision. The calculated distributions of $W_{pA}(\nu)$ for proton-lead interactions at three different energies are presented in the right panel of Fig. 2. They were calculated

in the framework of the Multiple Scattering Theory as

$$W_{pA}(\nu) = \sigma^{(\nu)} / \sigma_{prod}^{pA}, \quad (5)$$

where

$$\sigma^{(\nu)} = \frac{1}{\nu!} \int d^2b \cdot [\sigma_{inel}^{pN} \cdot T(b)]^\nu \cdot e^{-\sigma_{inel}^{pN} \cdot T(b)} \quad (6)$$

coincides [23, 24, 25, 26] with the optical model expression [27], and

$$\sigma_{prod}^{pA} = \int d^2b \cdot (1 - e^{-\sigma_{inel}^{pN} \cdot T(b)}), \quad (7)$$

with $T(b)$ being the profile function of the nuclear target:

$$T(b) = A \int_{-\infty}^{\infty} dz \cdot \rho(b, z), \quad (8)$$

where $\rho(r = \sqrt{b^2 + z^2})$ is the one-particle nuclear density.

The average value of ν has the well-known form:

$$\langle \nu \rangle = \frac{A \cdot \sigma_{inel}^{pp}}{\sigma_{prod}^{pA}}. \quad (9)$$

We use the values $\sigma_{inel}^{pp} = 72$ mb and $\sigma_{prod}^{pPb} = 1900$ mb at $\sqrt{s} = 5$ TeV, so the numerical value of $\langle \nu \rangle_{pPb}$ turns out to be of about 7.9.

In the calculation of the inclusive spectra of secondaries produced in pA collisions we should consider the possibility of one or several Pomeron cuts in each of the ν blobs of proton-nucleon inelastic interactions. For example, in Fig. 3 it is shown one of the diagrams contributing to the inelastic interaction of a beam proton with two lead nucleons. In the blob of the proton-nucleon1 interaction one Pomeron is cut, and in the blob of the proton-nucleon2 interaction two Pomerons are cut. It is essential to take into account all digrams with every possible Pomeron configuration and its permutations. The diquark and quark distributions and the fragmentation functions here are the same as in the case of the interaction with one nucleon.

In particular, the contribution of the diagram in Fig. 3 to the inclusive spectrum is

$$\begin{aligned} \frac{x_E}{\sigma_{prod}^{pA}} \cdot \frac{d\sigma}{dx_F} &= 2 \cdot W_{pPb}(2) \cdot w_1^{pN_1} \cdot w_2^{pN_2} \cdot \left\{ f_{qq}^h(x_+, 3) \cdot f_q^h(x_-, 1) + \right. \\ &+ f_q^h(x_+, 3) \cdot f_{qq}^h(x_-, 1) + f_s^h(x_+, 3) \cdot [f_{qq}^h(x_-, 2) + f_q^h(x_-, 2) + \\ &+ 2 \cdot f_s^h(x_-, 2)] \left. \right\}. \end{aligned} \quad (10)$$

The process shown in Fig. 3 satisfies [23, 24, 25, 26] the condition that the absorptive parts of the hadron-nucleus amplitude are determined by the combination of the absorptive parts of the hadron-nucleon amplitudes.

Sometimes, in the case of hadron-nucleus collisions the values of x_F have to be rescaled [28, 29] to account for the part of the initial energy that is used for nucleus desintegration, though this correction becomes negligibly small at LHC energies.

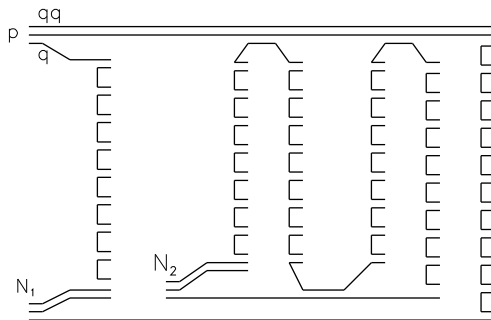


Figure 3: One of the diagrams contributing to the inelastic interaction of an incident proton with two target nucleons N_1 and N_2 in a pA collision.

3 Inclusive spectra in $p+A$ collisions at very high energy and inelastic screening (percolation) effects

The QGSM gives a reasonable description [2, 10, 30] of the inclusive spectra of different secondaries produced in hadron-nucleus and deuteron-nucleus collisions at energies $\sqrt{s_{NN}} = 14-30$ GeV. Also the experimental data of secondaries produced in Pb+Pb collisions at $\sqrt{s_{NN}} = 17$ GeV [31, 32] were reasonably described (except for some problems with charged kaons) by a superposition model in [12].

At RHIC energies the situation drastically changed. The spectra of secondaries produced in pp collisions can be rather well described, but the RHIC experimental data for Au+Au collisions [33, 34] give clear evidence of the inclusive density saturation effects which reduce the inclusive density about two times in the central (midrapidity) region when compared to the predictions based on the superposition picture [35, 36, 37]. This reduction can be explained by the inelastic screening corrections connected to multipomeron interactions [1]. The effect is very small for integrated cross sections (many of them are determined only by geometry), but it is very important [1] for the calculations of secondary multiplicities and inclusive densities at high energies.

Following the estimations presented in reference [1], the RHIC energies are just of the order of magnitude needed to observe this effect. The inelastic screening can make [1] the inclusive density to decrease in the midrapidity region about two times at RHIC energies and about three times at LHC energies, with respect to the calculations without inelastic screening.

However, all estimations are model dependent. The numerical weight of the contribution of the multipomeron diagrams is rather unclear due to the many unknown vertices in these diagrams. The number of unknown parameters can be reduced in some models, and for example in reference [1] the Schwimmer model [38] was used for the numerical estimations.

Another approaches were used in [39], where the phenomenological multipomeron vertices of eikonal type were introduced for enhancement diagram summation. In [40]

the problem was considered in parton model, as elastic and inelastic splitting of parton ladders (EPOS model).¹

New calculations of inclusive densities and multiplicities in percolation theory both in pp [49, 50], and in heavy ion collisions [50, 51] are in good agreement with the experimental data in a wide energy region.

The percolation model also provides a reasonable description of the transverse momentum distribution (at low and intermediate p_T) including the Cronin effect and the behaviour of the baryon/meson ratio [52, 53, 54]. Most of the effects predicted by percolation can be seen as a direct consequence of the strong colour fields produced in the collision. This feature is common to other approaches as the Colour Glass Condensate [55, 56], where a p_T scaling is also obtained [57].

In the percolation approach one assumes that if two or several Pomerons overlap in transverse space, they fuse in only one Pomeron. When all quark-gluon strings (cut Pomerons) are overlapping, the inclusive density saturates, reaching its maximal value at a given impact parameter. This approach has only one free parameter η , called the percolation parameter

$$\eta = N_s \cdot \frac{r_s^2}{R^2} \cdot \langle r(y) \rangle , \quad (11)$$

with N_s the number of produced strings, r_s the string transverse radius, and R the radius of the overlapping area. The factor $\langle r(y) \rangle$ accounts for the fact that the parton density near the ends of the string is smaller than in the central region, where we fix $r(0) = 1$. At large rapidities we have N_s strings with different parton densities, $r_i(y)$, and

$$N_s \cdot \langle r(y) \rangle = \sum_{i=1}^{N_s} r_i(y) . \quad (12)$$

As a result, the bare inclusive density $dn/dy|_{bare}$ gets reduced, and we obtain

$$dn/dy = F(\eta) \cdot dn/dy|_{bare} , \quad (13)$$

with [58]

$$F(\eta) = \sqrt{\frac{1 - e^{-\eta}}{\eta}} . \quad (14)$$

In order to account for the percolation effects in the QGSM, it is technically more simple [2] to consider in the central region the maximal number of Pomerons n_{max} emitted by one nucleon. These Pomerons lead, after they are cutted, to the different final states. Then the contributions of all diagrams with $n \leq n_{max}$ are accounted for as at lower energies. The larger number of Pomerons $n > n_{max}$ also can be emitted obeying the

¹ Another (model dependent) possibility to estimate the contribution of the diagrams with Pomeron interaction comes [41, 42, 43, 44, 45] from percolation theory. The percolation approach and its previous version, the String Fusion Model [46, 47, 48] predicted the multiplicity suppression seen at RHIC energies, long before any RHIC data were taken.

unitarity constraint, but due to fusion in the final state (on the quark-gluon string stage) the cut of $n > n_{max}$ Pomerons results in the same final state as the cut of n_{max} Pomerons.

By doing this, all model calculations become rather simple and very similar to the percolation approach. The QGSM fragmentation formalism allows one to calculate the integrated over p_T spectra of different secondaries as the functions of rapidity and x_F .

In this scenario we obtain a reasonable agreement with the experimental data on the inclusive spectra of secondaries at RHIC energy (see [2] with $n_{max} = 13$).

The simplest assumption of this approach corresponding to the general approach of the Parton Model [59, 60] is that of neglecting the energy dependence of n_{max} , i.e. of using a fixed $n_{max} = 13$ at LHC energy. However the numerical calculations [61] result in too strong shadow effects, and they are in contradiction with the measurements by the ALICE Collaboration [3].

On the other hand, it has been shown in [62] that the number of strings that can be used for the secondary production should increase with the initial energy. Thus, in the following calculations we use the value $n_{max} = 13$ at the LHC energy $\sqrt{s} = 5$ TeV, that can be considered as the normalization to ALICE data for all charged secondaries. The predictive power of our calculation applies for different sorts of secondaries in midrapidity region, as well as the calculations in the fragmentation region.

This scheme seems closer to the point of view of the Parton Model [59, 60], the numerical difference between the present scheme and [59, 60] coming from the fact that the ratio r_s^2/R^2 in Eq. (11) is rather small [2], so the percolation parameter, η , is also small at not very high energies and many $n \leq n_{max}$ independent Pomerons can exist before percolation plugs in. That explains why the effects of Pomeron (secondary particle) density saturation are small at fixed target energies and they become visible only starting from RHIC energies. The similar energy dependence in the Reggeon calculus [1] is connected to the suppression of the diagrams with multipomeron interactions due to the nuclear longitudinal form factor.

In the following calculations one additional effect is also accounted for, namely the transfer of the baryon charge to large distances in rapidity distances through the string junction effect [8, 63, 64, 65, 66, 67, 68]. This effect leads to an asymmetry in the production of baryons and antibaryons in the central region, that is non-zero even at LHC energies [69]. In the calculations of these effects we use the following values of the parameters [67]:

$$\alpha_{SJ} = 0.5 \quad \text{and} \quad \varepsilon = 0.0757. \quad (15)$$

4 Rapidity spectra of secondaries at LHC energies

In the lead-nucleus fragmentation region the contributions of intranuclear cascade and/or Fermi-motion of bound nucleons exist. To avoid these contributions we consider only the central (midrapidity) and the proton beam fragmentation regions.

The results of our calculations for the pseudorapidity density of all charged secondaries $dn_{ch}/d\eta$ is presented in Fig. 4. The calculations are normalized to the ALICE experimental point [3] $dn_{ch}/d\eta = 16.81 \pm 0.71$ measured in the window $|\eta_{lab}| \leq 2$. For comparison we also present the distribution $dn_{ch}/d\eta$ at the same energy.

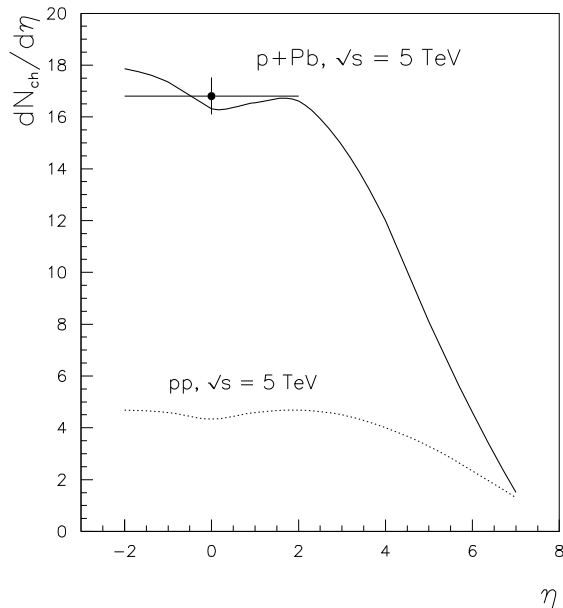


Figure 4: Pseudorapidity distributions for all charged secondaries produced in p+Pb collisions at $\sqrt{s_{NN}} = 5$ TeV (solid curve) with inelastic screening (percolation) corrections, normalized to the ALICE experimental point [3]. The dotted curve shows the QGSM predictions for pp collisions at $\sqrt{s_{NN}} = 5$ TeV.

It seems more suitable to discuss the spectra behaviour in terms of c.m. rapidity dn/dy_{cm} . The rapidity distributions of all charged secondaries dn_{ch}/dy_{cm} , where y_{cm} is determined in the frame of a incident proton interaction with one lead nucleon, calculated in the QGSM are presented on the left panel of Fig. 5. The solid curve shows the results obtained by accounting for the inelastic screening (percolation) corrections, the dashed curve shows the results obtained without these corrections, and the QGSM predictions for pp collisions at $\sqrt{s_{NN}} = 5$ TeV are presented by the dotted curve.

In the right panel of Fig. 5 we present the predictions for the nuclear modification factor

$$R_{ch}(y_{cm}) = \frac{dn_{ch}/dy_{cm}(pPb)}{dn_{ch}/dy_{cm}(pp)}. \quad (16)$$

Here again, the solid curve shows the QGSM predictions when accounting for the inelastic screening and the dashed curve corresponds to the results without these corrections.

In Fig. 5 one can clearly see that the values of dn_{ch}/dy , as well as those of the ratios $R_{ch}(pPb/pp)$, differ in the midrapidity region for about 1.7 times between the calcula-

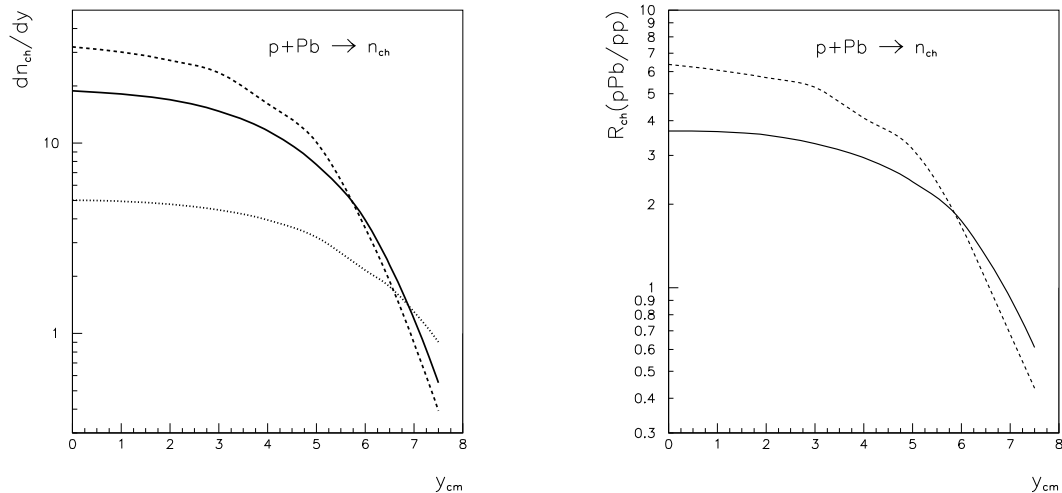


Figure 5: Rapidity distributions (left panel) and nuclear modification factors (right panel) for all charged secondaries produced in p+Pb collisions at $\sqrt{s_{NN}} = 5$ TeV. Dashed curves show the QGSM predictions without inelastic screening (percolation) corrections, solid curves show the QGSM predictions with these corrections, and the dotted curve in the left panel shows the QGSM predictions for pp collisions at $\sqrt{s_{NN}} = 5$ TeV.

tions with and without percolation effects, what is in agreement with the predictions in reference [1]. These differences decrease with rapidity, and at large y_{cm} , i.e. in the fragmentation region, $y_{c.m.} \geq 6.5$ these differences change sign, the values $R_{ch}(pPb/pp)$ becoming smaller than unity in agreement with the nuclear shadowing in the inclusive spectra [10, 11, 70].

The effect of the nuclear shadowing at large rapidities differs for about 1.5 times for the calculations with and without percolation effects, what is a direct consequence of energy conservation. The behaviour of the spectra in the proton fragmentation region is discussed in more detail in the next section.

The results of similar calculations for secondary protons are shown in Fig. 6. Here again, the difference in the predictions in the midrapidity region for the calculations with and without percolation effects is of about 1.7 times, and these differences decrease with rapidity. The rather complicate behaviour of the spectra in the fragmentation region is also discussed in the next section.

The calculated results of dn/dy_{cm} distributions for secondary Λ and $\bar{\Lambda}$ are shown in the upper panels of Fig. 7. The nuclear modification factors $R_{\Lambda}(pPb/pp)$ and $R_{\bar{\Lambda}}(pPb/pp)$ practically coincide inside the 10–15% accuracy margin, and they are presented in the lower panel of Fig. 7.

As a result, we can predict very similar behaviour of the nuclear modification factors for different secondaries in the midrapidity region and similar dependences of these factors on y_{cm} before the proton fragmentation regio, say until $R(pPb/pp) \geq 1$. At the

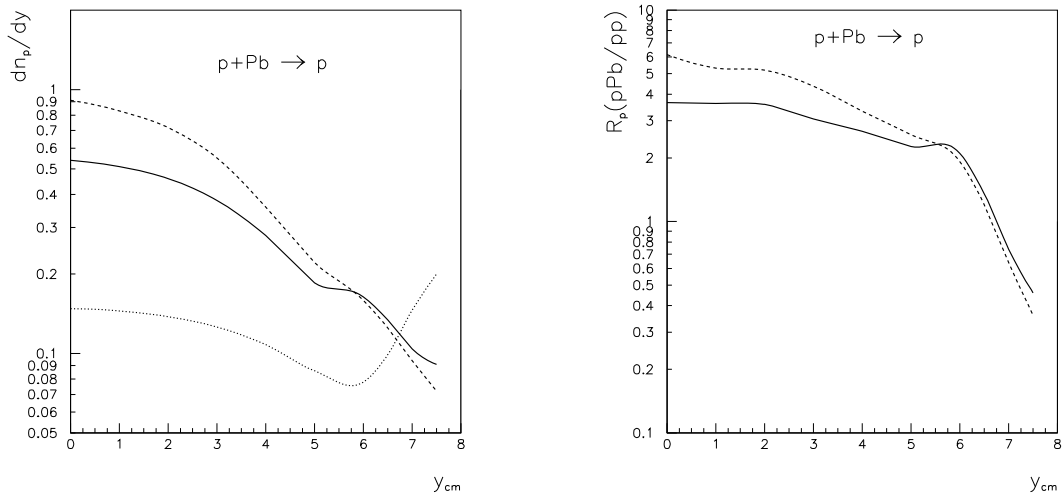


Figure 6: Rapidity distributions (left panel) and nuclear modification factors (right panel) for secondary protons produced in p+Pb collisions at $\sqrt{s_{NN}} = 5$ TeV. The correspondence of the curves is the same as in Fig. 5.

same time, these factors are about 1.7 times different at small $y - c.m.$ when they are calculated with and without inelastic screening corrections.

5 Feynman- x spectra at LHC energies

The x_F variable is mainly suited for the consideration of the inclusive spectra in the fragmentation region. For the case of the distributions $(x_E/\sigma_{inel}) \cdot (d\sigma/dx_F)$, x_F is determined in the c.m. frame of the interaction of an incident proton with one lead nucleon.

The distributions $(x_E/\sigma_{inel}) \cdot (d\sigma/dx_F)$ calculated in the QGSM are presented in the left panel of Fig. 8. The solid curve shows the result obtained with accounting for the inelastic screening (percolation) corrections, the dashed curve represents the result without these corrections, and the QGSM predictions for pp collisions at $\sqrt{s_{pp}} = 5$ TeV are presented by the dotted curve.

In the right panel of Fig. 8 we present the predictions for the nuclear modification factor

$$R_{ch}(x_F) = \frac{(1/\sigma_{prod}) \cdot (d\sigma_{ch}/dx_F)_{pPb}}{(1/\sigma_{inel}) \cdot (d\sigma_{ch}/dx_F)_{pp}} \quad (17)$$

Here again, the solid curve shows the QGSM predictions with accounting for the inelastic screening and dashed curve shows the result without these corrections.

The results of the corresponding calculations for the secondary protons are shown in Fig. 9, where the effects of nuclear shadowing in the fragmentation region are very clearly seen, being about 1.5 times different at $x_F \geq 1/2$ for the calculations with and

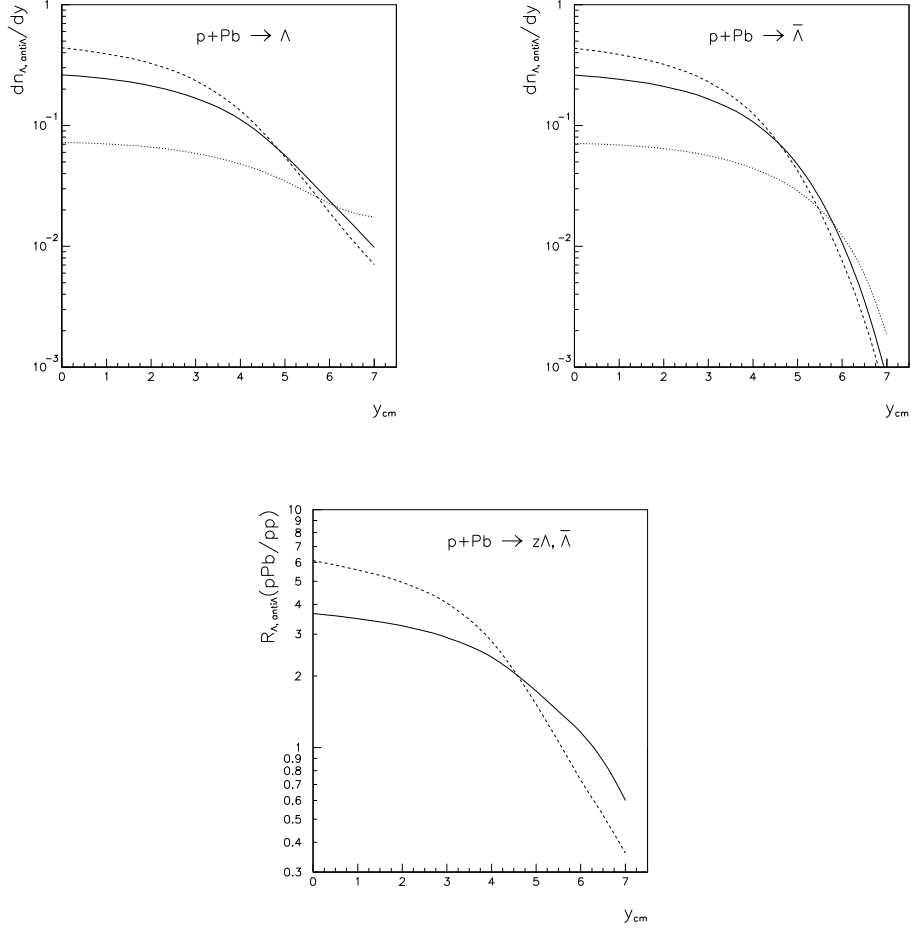


Figure 7: Rapidity distributions for secondary Λ (left up) and $\bar{\Lambda}$ (right up) produced in p+Pb collisions at $\sqrt{s_{NN}} = 5$ TeV, and the corresponding nuclear modification factors for them (low). The correspondence of the curves is the same as in Fig. 5.

without percolation effects.

Some predictions of the nuclear shadowing in the fragmentation region were obtained [70] in the framework of the Additive Quark Model (AQM). In this model the fast baryon is considered as formed by three constituent quarks, each carrying out around 1/3 of the total baryon momentum (sea quarks and gluons are assumed to be effectively included inside the constituent quarks). Let a secondary baryon with $x_F \sim 2/3$ to be formed by two constituent quarks from the initial baryon, the examples being the reactions $p \rightarrow p$, $p \rightarrow \Lambda$, etc. The simplest mechanism in the framework of AQM to get this is the recombination of two quark-spectators of the incident baryon with one newly produced quark from the sea.

The A-dependence of such a processes is determined by the probability to have two quark-spectators in pA collisions. If the constituent quarks interact with the target

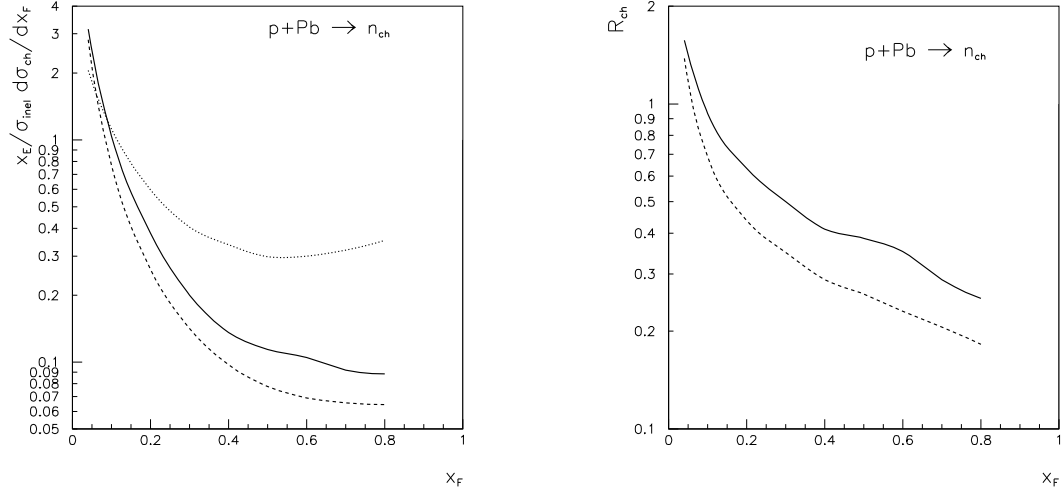


Figure 8: Feynman- x distributions (left panel) and nuclear modification factors $R_{ch}(x_F)$ (right panel) for all charged secondaries produced in p+Pb collisions at $\sqrt{s_{NN}} = 5$ TeV. The correspondence of the curves is the same as in Fig. 5.

independently, the cross section of their inelastic interaction with a proton target is

$$\sigma_{inel}^{qN} = \frac{1}{3} \cdot \sigma_{inel}^{NN} , \quad (18)$$

and the probability that one constituent quark will interact with the target nucleus while two other constituent quarks are spectators can be written as:

$$V_1^{pA} = \frac{3}{\sigma_{prod}^{pA}} \cdot \int d^2b \cdot e^{-2\sigma_{inel}^{qN} \cdot T(b)} \cdot [1 - e^{-\sigma_{inel}^{qN} \cdot T(b)}] , \quad (19)$$

where $T(b)$ is determined by Eq. (8).

The AQM predicts an A dependence

$$R_{p,n,\Lambda,\dots}(x_F \sim 2/3) = V_1^{pA} , \quad (20)$$

and such a simple relation is actually in good agreement [11, 70, 71] with the experimental data.

The AQM prediction from Eq. (20) is shown in the right panel of Fig. 9 by a dash-dotted straight line, and it is in agreement with the QGSM calculation without inelastic shadow corrections. Shadow corrections (elastic as well as inelastic ones) also exist in the AQM but they are not accounted for in eqs. (18) and (19).

The calculated results for the Λ -hyperon production $(x_E/\sigma_{inel}) \cdot (d\sigma_\Lambda/dx_F)$ distributions, and the corresponding nuclear modification factors $R_\Lambda(x_F)$, are shown in Fig. 9, where the AQM prediction from Eq. (20) is presented in the right panel of Fig. 10 by the dash-dotted straight line.

In Fig. 10 one can clearly appreciate that the spectra of $\bar{\Lambda}$ at large x_F are very small.

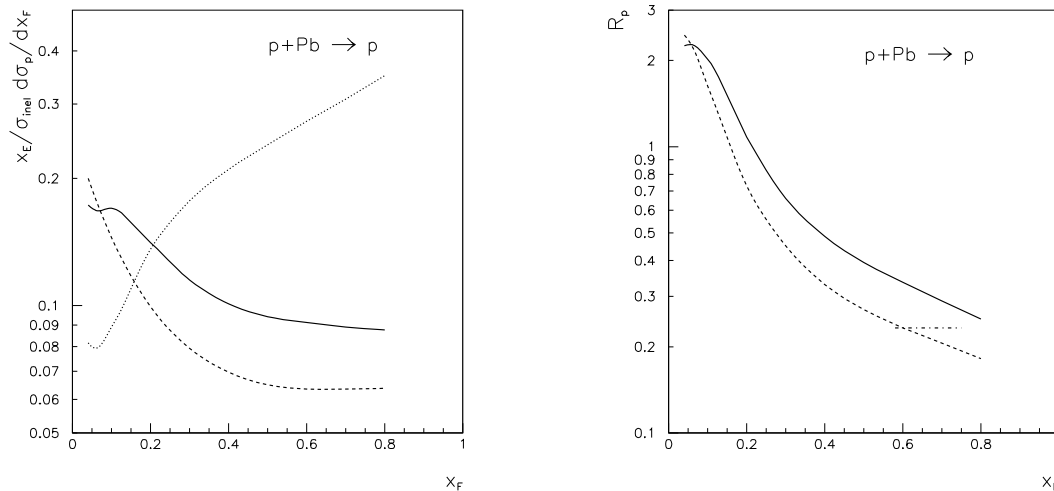


Figure 9: Feynman- x distributions (left panel) and nuclear modification factors (right panel) for secondary protons produced in p+Pb collisions at $\sqrt{s_{NN}} = 5$ TeV. The correspondence of the curves is the same as in Fig. 5. The AQM predictions (eqs. (19) and (20)) are shown by the dash-dotted straight line.

6 Conclusions

The percolation (inelastic screening) effects are too small to be observed by comparing the model calculations to experimental data at fixed target energies $\sqrt{s_{NN}} = 15\text{--}40$ GeV. At RHIC energies, these effects in $dn_{ch}/dy(y=0)$ become to be a factor of about 1.5 [2], and they can increase up to a factor 1.7 at the LHC energy, i.e. a rather slow increase with energy. A so significant effect at the LHC energies is connected to the fact that at $\sqrt{s_{NN}} = 5$ TeV, $\langle n_{NN} \rangle \sim 3$ and $\langle \nu_{NPb} \rangle \sim 8$, so the average value of Pomerons (~ 24) in the minimum bias p+Pb collision is of the same order as $n_{max} = 25$, and for larger number of Pomerons (quark-gluon strings) the fusion processes become very important. These processes decrease the inclusive densities (nuclear modification factors $R(y_{cm})$ of Eq. (16)) in the midrapidity region.

Due to the same reason the inclusive densities (the ratios $R(x_F)$ of Eq. (17)) in the fragmentation region should increase. Here we predict the disagreement with the AQM results.

The detailed experimental confirmation of the inelastic screening (percolation) effects for the inclusive spectra can be considered as a natural “bridge” between the mechanisms of the hadron density saturation in soft and hard processes.

The point to be stressed is the energy dependence [62] of n_{max} from RHIC to LHC energies, and this dependence should be reproduced when computing the enhancement Reggeon diagrams.

Our results are in reasonable numerical agreement with those in ref. [72].

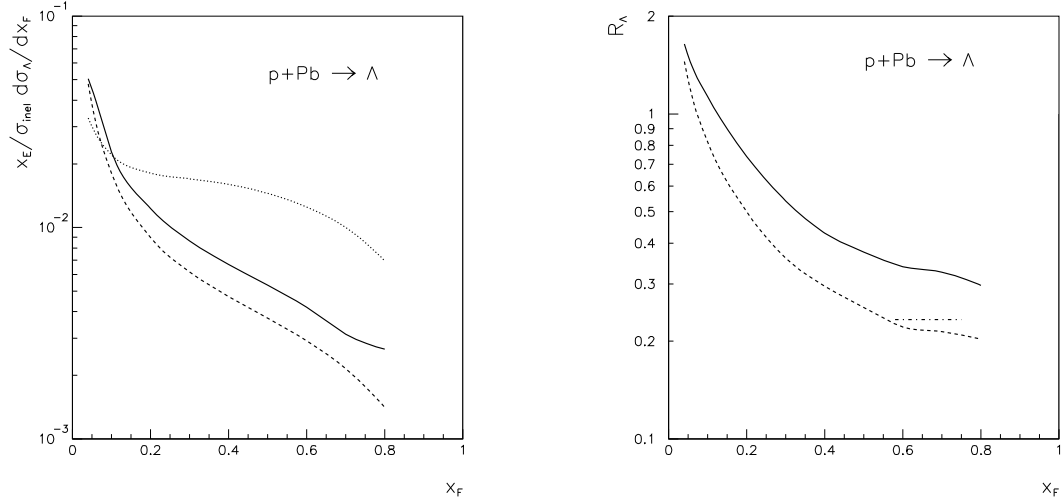


Figure 10: Feynman- x distributions (left) and nuclear modification factors (right) for secondary Λ produced in p+Pb collisions at $\sqrt{s_{NN}} = 5$ TeV. The correspondence of the curves is the same as in Fig. 5. The AQM predictions from eqs. (19) and (20) are shown by a dash-dotted straight line.

Acknowledgements

We are grateful to N. Armesto and J. Dias de Deus for useful discussions. This paper was supported by Ministerio Educación y Ciencia of Spain under project FPA 2011-22776, by the Spanish Consolider CPAN Project, and by Xunta de Galicia (Spain) and, in part, by the grant RFBR 11-02-00120-a.

References

- [1] A. Capella, A. Kaidalov, and J. Tran Thanh Van, *Heavy Ion Phys.* **9**, 169 (1999).
- [2] C. Merino, C. Pajares, and Yu.M. Shabelski, *Eur. Phys. J.* **C59**, 691 (2009) and arXiv:0802.2195 [hep-ph].
- [3] ALICE Collaboration, arXiv:1210.3615 [nucl-ex].
- [4] A.B. Kaidalov and K.A. Ter-Martirosyan, *Yad. Fiz.* **39**, 1545 (1984); **40**, 211 (1984).
- [5] A.B. Kaidalov, *Phys. Atom Nucl.* **66**, 1994 (2003).
- [6] A. B. Kaidalov and O. I. Piskunova, *Yad. Fiz.* **41**, 1278 (1985).
- [7] Yu.M. Shabelski, *Yad. Fiz.* **44**, 186 (1986).
- [8] G.H. Arakelyan, A. Capella, A.B. Kaidalov, and Yu.M. Shabelski, *Eur. Phys. J.* **C26**, 81 (2002) and hep-ph/0103337.

- [9] G.H. Arakelyan, C. Merino, C. Pajares, and Yu.M. Shabelski, Eur. Phys. J. **C54**, 577 (2008) and arXiv:/0709.3174[hep-ph].
- [10] A.B. Kaidalov and K.A. Ter-Martirosyan, and Yu.M. Shabelski, Yad. Fiz. **43**, 1282 (1986).
- [11] Yu.M. Shabelski, Z. Phys. **C38**, 569 (1988).
- [12] J. Dias de Deus and Yu.M. Shabelski, Yad. Fiz. **71**, 191 (2008); Phys. Atom. Nucl. **71**, 190 (2008).
- [13] J. Blejbel et al., arXiv:1011.2703[hep-ph].
- [14] K. Tywonuk et al., Int. J. Mod. Phys. **E16**, 2301 (20087).
- [15] N. Armesto et al., J. Phys. **CG35**, 054001 (2008) and arXiv:0711.0974[hep-ph].
- [16] N. Armesto, arXiv:0903.1330[hep-ph].
- [17] C.A. Salgado et al., J. Phys. **G39**, 015010 (2012) and arXiv:1105.2919[hep-ph].
- [18] G.G. Barnafoldi et al. Phys. Rev. **C85**, 024903 (2012) and arXiv:1111.3646[nucl-th].
- [19] V.A. Abramovsky, V.N. Gribov, and O.V. Kancheli, Yad. Fiz. **18**, 595 (1973).
- [20] A.B. Kaidalov, Sov. J. Nucl. Phys. **45**, 902 (1987); Yad. Fiz. **43**, 1282 (1986).
- [21] M. Hladik et al., Phys. Rev. Lett. **86**, 3506 (2001).
- [22] K.A. Ter-Martirosyan, Phys. Lett. **44B**, 377 (1973).
- [23] Yu.M. Shabelski, Yad.Fiz. **26**, 1084 (1977); Nucl. Phys. **B132**, 491 (1978).
- [24] L. Bertocchi and D. Treleani, J. Phys. **G3**, 147 (1977).
- [25] J. Weis, Acta Phys. Polonica **B7**, 85 (1977).
- [26] T. Jaroszewicz et al., Z. Phys. **C1**, 181 (1979).
- [27] J.S. Trefil and F. von Hippel, Phys. Rev. **D7**, 2000 (1973).
- [28] Ya.A. Berdnikov, M.M. Ryzhinskiy, and Yu.M. Shabelski, Phys. Atom. Nucl. **69**, 1330 (2006).
- [29] Ya.A. Berdnikov, M.M. Ryzhinskiy, and Yu.M. Shabelski, Phys. Atom. Nucl. **70**, 732 (2007).
- [30] Yu.M. Shabelski, Sov. J. Nucl. Phys. **45**, 143 (1987); Z. Phys. **C38**, 569 (1988).

- [31] NA49 Collaboration (F. Sikler et al.), Nucl. Phys. **C661**, 45c (1999).
- [32] NA49 Collaboration (S.V. Afanasiev et al.), Phys. Rev **C66**, 054902 (2002) and nucl-ex/0205002.
- [33] PHOBOS Collaboration (B.B. Back et al.), Phys. Rev. Lett. **85**, 3100 (2000).
- [34] PHENIX Collaboration (K. Adcox et al.), Phys. Rev. Lett. **86**, 500 (2001).
- [35] A. Capella, C. Merino and J. Tran Thanh Van, Phys. Lett. **B265** (1991) 415.
- [36] Yu.M. Shabelski, Z. Phys. **C57**, 409 (1993).
- [37] N. Armesto and C. Pajares, Int. J. Mod. Phys. **A15**, 2019 (2000).
- [38] A. Schwimmer, Nucl. Phys. **B94**, 445 (1975).
- [39] S. Ostapchenko, Phys. Rev. **D77**, 034009 (2008).
- [40] K. Werner, Fu-Ming Liu, and T. Pierog, Phys. Rev. **C74**, 0449902 (2006).
- [41] J. Dias de Deus, R. Ugoccioni, and A. Rodrigues, Phys. Lett. **B458**, 402 (1999).
- [42] J. Dias de Deus, R. Ugoccioni, and A. Rodrigues, Eur. Phys. J. **C16**, 537 (2000).
- [43] M.A. Braun and C. Pajares, Phys. Rev. Lett. **85**, 4864 (2000).
- [44] J. Dias de Deus and Yu.M. Shabelski, Eur. Phys. J. **A20**, 457 (2004).
- [45] P. Brogueira, J. Dias de Deus, and C. Pajares, Phys. Rev. **C75**, 054908 (2007).
- [46] C. Merino, C. Pajares, and J. Ranft, Phys. Lett. **276**, 168 (1992).
- [47] H.J. Möhring, J. Ranft, C. Merino, and C. Pajares, Phys. Rev. **D47**, 4142 (1993).
- [48] N.S. Amelin, M.A. Braun, and C. Pajares, Z. Phys. **C63**, 507 (1994).
- [49] I. Bautista, C. Pajares, and J. Dias de Deus, Nucl. Phys. **A882**, 44 (2012).
- [50] I. Bautista, J. Dias de Deus, G. Milhano, and C. Pajares, Phys. Lett. **B715**, 230 (2012).
- [51] I. Bautista, C. Pajares, G. Milhano, and J. Dias de Deus, Phys. Rev. **C86**, 034909 (2012).
- [52] J. Dias de Deus, E. G. Ferreira, C. Pajares, and R. Ugoccioni, Eur. Phys. J. **C40**, 229 (2005).
- [53] C. Pajares, Eur. Phys. J. **C43**, 9 (2005).

- [54] L. Cunqueiro, J. Dias de Deus, E. G. Ferreira, and C. Pajares, *Eur. Phys. J.* **C53**, 585 (2008).
- [55] L.D. McLerran and R. Venugopalan, *Phys. Rev.* **D49**, 2233 (1994).
- [56] E.G. Ferreira, E. Iancu, A. Leonidov, and L.D. McLerran, *Nucl. Phys.* **A703**, 489 (2002).
- [57] J. Schaffner-Bielich, D. Kharzeev, L.D. McLerran, and R. Venugopalan, *Nucl. Phys.* **A705**, 494 (2002).
- [58] M.A. Braun and C. Pajares, *Eur. Phys. J.* **C16**, 2019 (2000).
- [59] O.V. Kancheli, *JETP Lett.* **18**, 274 (1973).
- [60] G.V. Davidenko and N.N. Nikolaev, *Yad. Fiz.* **24**, 772 (1976).
- [61] C. Merino, C. Pajares, and Yu.M. Shabelski, arXiv:1207.6900 [hep-ph].
- [62] J. Dias de Deus and C. Pajares, *Phys. Lett.* **B695**, 211 (2012) and arXiv:1011.1099[hep-ph].
- [63] X. Artru, *Nucl. Phys.* **B85**, 442 (1975).
- [64] M. Imachi, S. Otsuki, and F. Toyoda, *Prog. Theor. Phys.* **52**, 346 (1974); **54**, 280 (1976); **55**, 551 (1976).
- [65] G.C. Rossi and G. Veneziano. *Nucl. Phys.* **B123**, 507 (1977).
- [66] D. Kharzeev. *Phys. Lett.* **B378**, 238 (1996).
- [67] C. Merino, M.M. Ryzhinskiy, and Yu.M. Shabelski, *Eur. Phys. J.* **B62**, 491 (2009).
- [68] F. Bopp and Yu.M. Shabelski, *Eur. Phys. J. A* **28**, 237 (2006) and hep-ph/0603193.
- [69] C. Merino, C. Pajares, M.M. Ryzhinskiy, and Yu.M. Shabelski, arXiv:1007.3206 [hep-ph].
- [70] V.V. Anisovich, Yu.M. Shabelski, and V.M. Shekhter, *Nucl. Phys.* **B133**, 477 (1978).
- [71] V.V. Anisovich and Yu.M. Shabelski, *Sov. J. Nucl. Phys.* **34**, 462 (1981).
- [72] A. Dumitru, D. Kharzeev, E.M. Levin, and Y. Nara. *Phys. Rev.* **C85**, 044922 (2012).